Research Article

Journal of Environmental Nanotechnology

Bio-derived Kraft Lignin as a Green Stabilizer for Surfactant-assisted Nanosilica Dispersion in Cementitious Systems

J. Vignesh[1], Vidhya Lakshmi Sivakumar[1*], A. Kandasamy[1] and Mahmoud Al Khazaleh[2]

[1]Department of Civil Engineering, Saveetha School of Engineering, Saveetha Institute of Medical and Technical Sciences, Chennai, TN, India
[2]Department of Civil Engineering, Dean of Munib and Angela Masri Engineering Faculty Aqaba University of Technology, AQ, Jordan
Received: 03.08.2025 Accepted: 25.09.2025 Published: 30.09.2025
*vidhyalakshmis.sse@saveetha.com

ABSTRACT

This work explores the potential of Kraft Lignin-modified nanosilica (KL–NS) as a sustainable additive for cementitious composites, comparing its performance with both PCE-based nanosilica and plain OPC. The investigation combined microstructural analysis of pore features and hydration products with macro-scale measurements of compressive strength, ultrasonic pulse velocity (UPV), and electrical resistivity, supported by statistical validation. The inclusion of KL–NS led to a denser, more homogeneous matrix by accelerating hydration, consuming portlandite, and promoting greater C–S–H gel formation. Clear refinements in pore structure were observed: compared to OPC, the critical, average, and median pore diameters decreased by about 31–32%, while total porosity dropped by 21%. Even when benchmarked against PCE–NS, the KL–NS blends displayed a finer pore network and lower porosity, underlining its effectiveness in dispersing nanosilica and stabilizing hydration products. These structural improvements translated into notable performance gains. At 90 days, compressive strength rose to 58.2 MPa, representing increases of 40% over OPC and 9% over PCE–NS. UPV and resistivity also climbed to 5480 m/s and 27.8 kΩ·cm, which were 41% and 41.1% higher than OPC, respectively. All differences were statistically significant ($P < 0.001$). Alongside these technical benefits, Kraft Lignin's renewable and bio-based nature makes it as an eco-friendly substitute for synthetic dispersants, offering a path toward more durable and sustainable cementitious composites.

Keywords: Kraft Lignin; Nanosilica; Pore structure refinement; Compressive strength; Electrical resistivity; Hydration enhancement.

1. INTRODUCTION

Cement-based composites are extensively used in construction due to their low cost, abundant raw materials, and favorable properties, including high compressive strength, stiffness, and long-term durability (Zhang *et al*. 2016; Hossain *et al*. 2016; Puttbach *et al*. 2024). Nevertheless, these materials are inherently brittle, exhibit low tensile capacity, and are susceptible to degradation under aggressive environmental conditions, which can reduce structural lifespan and increase maintenance requirements (Kaewunruen *et al*. 2018; Baten *et al*. 2021; Karamloo *et al*. 2016). To address these limitations, integrating nanomaterials into cementitious systems has gained increasing attention. Their high surface area and reactivity enable modifications at the micro- and nanoscale, improving hydration kinetics, refining the microstructure, and enhancing mechanical performance and durability (Paul *et al*. 2018; Huseien *et al*. 2023; Shah *et al*. 2015; Kandasamy *et al*. 2025a; Sabari *et al*. 2025).

Among nanomaterials, nanosilica (NS) is widely explored due to its amorphous structure, fine particle size (5–100 nm), large surface area, and abundant surface hydroxyl groups, which facilitate pozzolanic reactions and C–S–H gel formation (Quercia *et al*. 2013; Haruehansapong *et al*. 2014; Al-Abboodi *et al*. 2020; Mahmood *et al*. 2022; Xu *et al*. 2016; Rupasinghe *et al*. 2017). Incorporating NS into cement matrices improves early-age strength, densifies the microstructure, and reduces porosity, while sol-based NS has shown superior dispersion and reactivity compared to dry powders (Farjad *et al*. 2025; Chen *et al*. 2024). Nanosilica has also been applied in high-strength self-compacting concretes to counteract strength loss at elevated temperatures and optimize mechanical performance, with smaller particles (~10 nm) achieving greater benefits (Pooja *et al*. 2024; Alam *et al*. 2024).

Despite its benefits, NS faces dispersion challenges in highly alkaline cement pore solutions, where OH^-, Na^+, K^+, and Ca^{2+} ions promote particle agglomeration and reduce reactivity (Yang *et al*. 2023). Conventional dispersants, such as polycarboxylate ether

(PCE), are commonly used to stabilize NS, often combined with ultrasonication, but they have environmental and economic drawbacks (Ren *et al*. 2020; Iqbal *et al*. 2024). These limitations highlight the need for sustainable alternatives that can maintain NS dispersion while enhancing performance.

Kraft lignin (KL), a natural polymer produced as a by-product of the paper industry, has emerged as a promising green dispersant. Its aromatic structure and functional groups (hydroxyl, methoxyl, and carboxyl) enable strong interactions with NS particles and cement phases, preventing agglomeration and promoting uniform distribution (Zandonadi *et al*. 2024; Kandasamy *et al*. 2025c; Argyropoulos *et al*. 2023; Dessbesell *et al*. 2020). Its amphiphilic character allows it to act as a compatibilizer in composite systems, while its renewable origin aligns with circular economy principles. In cementitious systems, kraft lignin has been shown to improve water retention, reduce segregation, and enhance microstructural densification (Gupta *et al*. 2015; Rajagopalan *et al*. 2022).

This study investigates the effects of kraft lignin-stabilized NS on cementitious composites in comparison with PCE-dispersed NS and plain OPC. Microstructural characterization was performed using X-ray diffraction (XRD) to monitor hydration products (Seong-Seok *et al*. 2010), thermogravimetric analysis (TGA) for phase quantification, mercury intrusion porosimetry (MIP) for pore structure, and scanning electron microscopy (SEM) for morphology. Macroscopic performance was evaluated through compressive strength, ultrasonic pulse velocity (UPV), and electrical resistivity at various curing ages. Furthermore, the environmental and economic implications of using Kraft lignin were considered relative to conventional PCE, emphasizing its potential as a sustainable, high-performance dispersant for cementitious systems.

2. EXPERIMENTAL METHODOLOGY

2.1 Materials Used

For this study, Ordinary Portland Cement (OPC) of 43 Grade, conforming to IS 8112:2013, was used. The cement had a density of 3.15 g cm^{-3} and a Blaine fineness of 3450 cm^2/g^{-1}. The nano silica (NS) selected was an amorphous silica nanopowder obtained from Sigma-Aldrich, with an average particle size in the range of 15–20 nm, a high specific surface area of around 200 m^2/g^{-1}, and a bulk density of 2.2 g cm^3. The morphology and dispersion characteristics of NS are illustrated in Fig. 1a, while its amorphous structure was verified by X-ray diffraction (XRD) analysis (Fig. 2), which agrees with earlier observations (Naddaf *et al.* 2020). The chemical oxide composition of both OPC and NS are summarized in Table 1. Furthermore, the mineralogical phases of OPC were calculated using the Bogue equations, and the corresponding values are listed in Table 2. For the fine aggregate, standard natural river sand was utilized, having a maximum particle size of 1.18 mm and a specific gravity of 2.65, in accordance with IS 650:1991 and IS 383:2016.

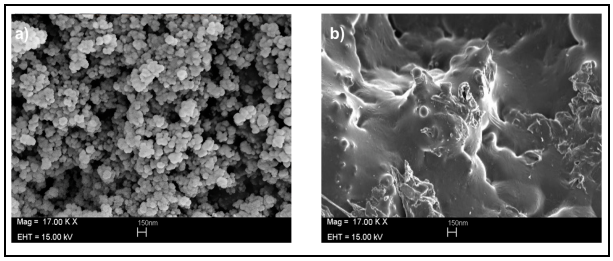


Fig. 1: SEM images of (a) nano silica and (b) kraft lignin

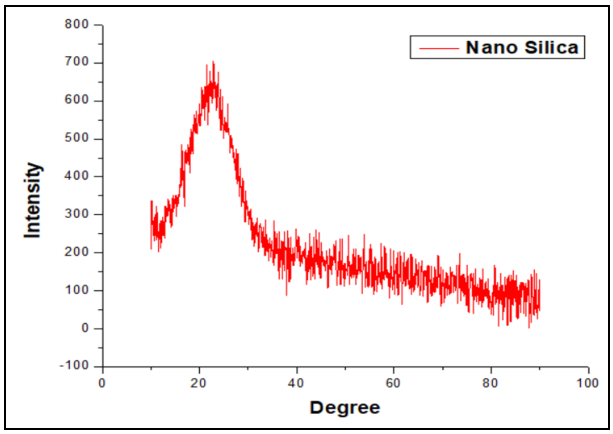


Fig. 1: XRD patterns of nano silica

To enhance the stability of NS dispersions in the highly alkaline cementitious medium, two types of dispersants were investigated. Kraft lignin, an industrial byproduct of the pulping process, was introduced as a sustainable bio-based modifier. Its complex macromolecular structure, enriched with phenolic and carboxylic groups, allows effective adsorption on nano silica surfaces, thereby reducing agglomeration through electrostatic repulsion and steric hindrance. This property makes Kraft lignin an attractive green alternative for promoting homogeneous nanoparticle distribution.

The morphology and dispersion state of kraft lignin are highlighted in Fig. 1b. For comparison, a PCE–based superplasticizer, commonly used in cementitious systems across India, was incorporated as a benchmark chemical dispersant. The physicochemical characteristics of Kraft lignin and PCE are presented in Table 3 to facilitate evaluation of their relative effectiveness in stabilizing NS dispersions within the cement matrix.

Table 1. Chemical composition of OPC and NS

Material	SiO_2	Al_2O_3	Fe_2O_3	CaO	MgO	SO_3	K_2O	Loss on Ignition (%)
OPC	21.5	4.8	3.1	63.2	2.5	2.6	0.8	1.5

Table 2. Mineral compositions of OPC

Mineral	Alite (C_3S)	Belite (C_2S)	Aluminate (C_3A)	Ferrite (C_4AF)
Content (wt. %)	52.0	23.0	7.5	8.5

Table 3. Surfactant characteristics used

Surfactant	Density (g/cm³)	Physical State	Color
Kraft Lignin	1.30–1.40	Powder (solid)	Brown to dark brown
PCE	1.01	Liquid (aqueous)	Clear yellow to amber

2.2 Kraft Lignin and PCE–NS Suspension Preparation

Kraft lignin–NS suspension was a combined physicochemical dispersion approach was employed. First, NS powder was dispersed in deionized water (pH ≈ 6.8) and ultrasonicated using a probe-type ultrasonic processor (400 W, 20 kHz) with a 13-mm titanium tip. The sonication process was carried out for 10 minutes in pulse mode (15 seconds on, 5 seconds off), while maintaining the suspension in an ice-cold water bath to minimize heat generation and prevent nanoparticle agglomeration. After sonication, Kraft lignin powder was introduced into the dispersion and blended using a high-speed mechanical stirrer at 1000 rpm for 2 minutes to ensure uniform mixing and adsorption of lignin molecules on the silica surface. For comparison, the PCE–NS suspension was prepared following established methods, where the PCE surfactant was directly added to the NS dispersion under the same sonication and mixing conditions.

2.3 Mix Design, Casting, and Curing Procedure

Cement mortar specimens were fabricated in three groups, as outlined in Table 4. The mix was prepared with a water-to-binder ratio of 0.485 and a sand-to-binder ratio of 2.5, where the binder comprised OPC and nano silica. The dosage of Kraft lignin or PCE surfactant was fixed at 0.3% by weight of the binder, in line with effective concentrations identified in earlier studies (Li *et al.* 2023; Qian *et al*. 2018). The prepared Kraft lignin-NS or PCE–NS suspensions were mixed with OPC and standard graded sand in a laboratory mortar mixer. The mixing protocol adhered to the IS 4031 (Part 6):1988 procedure, which is equivalent to ASTM C305. Fresh mortar was poured into 50 mm cube molds and 40 × 40 × 160 mm prism molds. The filled molds were placed on a standard vibrating table operating at 25 Hz for about 2 minutes to remove trapped air and achieve uniform compaction. After 24 hours of casting, the specimens were demolded and transferred to a curing chamber maintained at 27 ± 2 °C with relative humidity exceeding 95%. They were then immersed and kept under these conditions until the scheduled testing periods.

Table 4. Mix proportions of samples

Mix Code	OPC (kg/m³)	Nano-silica (kg/m³)	Water (kg/m³)	Standard Sand (kg/m³)	Kraft Lignin (% Binder Mass)	PCE (% Binder Mass)
CTRL	542.50	–	263.1	1 356.3	–	–
NS–KF	531.65	10.85	265.0	1 356.3	0.3 %	–
NS–PCE	531.65	10.85	263.1	1 356.3	–	0.3 %

2.4 Methods of Testing

2.4.1 Microscopic Characteristics

2.4.1.1 X-ray Diffraction (XRD)

The crystalline hydration products were analyzed using a PANalytical X'Pert PRO X-ray diffractometer fitted with a Ni-filtered Cu Kα radiation source (λ = 1.5406 Å). The scans were carried out over a 2θ range of 5°–60°, with a step size of 0.04°. For this purpose, powdered samples were taken from the core portion of 90-day cured cubes after compressive strength testing. The fragments were finely ground to pass through a 75 μm sieve (IS No. 200) and then oven-dried under vacuum at 25 ± 2 °C for 72 hours to remove residual moisture before subjecting them to XRD analysis.

2.4.1.2 Thermogravimetric Analysis (TGA)

Thermal decomposition and mass loss behavior, indicative of hydration and pozzolanic activity, were analyzed using a simultaneous thermal analyzer

(NETZSCH STA 449 F3 Jupiter, Germany), which enabled the combined measurement of thermogravimetric (TG) and differential scanning calorimetry (DSC) responses. Approximately 15 mg of finely ground cementitious paste from the 90-day nano silica-modified mortar specimens was subjected to a heating cycle from 50 °C to 1000 °C at a constant heating rate of 10 °C/min under an inert argon environment. Sample preparation followed the same drying and grinding procedures as used for the XRD tests.

2.4.1.3 Mercury Intrusion Porosimetry (MIP)

The pore characteristics and overall porosity of mortars cured for 90 days were evaluated using a mercury intrusion porosimeter (Quantachrome PoreMaster 60, USA). Test samples were obtained from fractured sections of compressive strength cubes and carefully trimmed to approximately 5 mm in size, with an average weight of about 0.8 g. To stop further hydration, the fragments were soaked in absolute ethanol for 24 hours, followed by vacuum drying at 25 ± 2 °C for 72 hours. The porosimeter applied pressures ranging from 0.01 MPa up to 420 MPa, enabling pore detection between ~120 µm and 3 nm. A contact angle of 130° and a mercury surface tension of 0.485 N/m were considered, with a stabilization period of 20 seconds maintained during each intrusion step.

2.4.1.4 Scanning Electron Microscopy (SEM)

The surface morphology and microstructural features of 90-day nano silica-modified mortars were visualized using a Hitachi S-4800 scanning electron microscope (Japan). Small specimens measuring roughly 5 × 5 × 2 mm^3 were extracted from fractured regions of compressive test specimens. Before imaging, all samples underwent vacuum drying at 23 ± 2 °C for 72 hours, followed by precision polishing and gold sputter-coating to enhance conductivity. The SEM was operated at an accelerating voltage of 20 kV, a beam spot size of 5.0, and a working distance of 10 ± 2 mm to obtain high-resolution micrographs of the cement matrix and particle distribution.

2.4.2 Macroscopic Characteristics

2.4.2.1 Compressive Strength

The compressive strength test was carried out on 50 mm cubic mortar specimens at the curing intervals of 28 and 90 days, using a calibrated compression testing machine with a maximum load capacity of 3000 kN and a loading rate of 1.5 kN/s, in accordance with IS 4031 (Part 6):1988, which specifies the procedure for determining compressive strength of cement mortar cubes. The specimens were tested under uniform loading conditions to assess strength development over time.

2.4.2.2 Ultrasonic Pulse Velocity (UPV)

Ultrasonic pulse velocity (UPV) measurements were carried out on prismatic mortar specimens of 40 × 40 × 160 mm, cured for 28 and 90 days. The tests were performed in accordance with IS 13311 (Part 1):1992, which provides guidelines for non-destructive assessment of concrete using ultrasonic pulses. A Proceq Pundit Lab+ device was used for the measurements, with both ends of each specimen coated with a thin layer of grease to ensure proper coupling between the transducer and receiver, allowing accurate transmission of acoustic waves.

2.4.2.3 Electrical Resistivity

The electrical resistivity of mortar specimens was measured at 28 and 90 days using the two-electrode technique, following the procedures outlined by Yim *et al*. 2017). Prismatic samples measuring 40 × 40 × 160 mm, in a saturated surface-dry condition, were placed between brass plate electrodes (60 × 60 × 1 mm). A 1 kHz alternating current (AC) signal was applied via a digital resistivity meter, and the resulting resistance was recorded. To improve contact between the electrodes and specimen surfaces, damp sponges were positioned at both ends. The bulk resistivity (ρ) was determined using the relationship:

$$\rho = (R \times A) / l \quad \ldots(1),$$

where ρ represents the electrical resistivity in kilo-ohm centimeters (kΩ·cm), R is the measured resistance in kilo-ohms (kΩ), A is the specimen's cross-sectional area in cm^2, and l is the electrode spacing in cm.

For all macroscopic and microscopic tests, six specimens per group were used for macroscopic measurements and three specimens per group for microscopic analyses. The results presented represent the average values calculated from these measurements.

3. EXPERIMENTAL RESULTS

3.1 Microscale Morphology

3.1.1 X-ray Diffraction (XRD) Analysis

The impact of PCE and KL admixtures on the crystalline phase evolution of nano-silica (NS) incorporated OPC composites, cured for 90 days, was systematically investigated through X-ray diffraction (XRD) analysis. The resulting diffractograms depicted in Fig. 3 provided compelling evidence of the distinct roles these organic admixtures play in modulating both primary cement hydration and secondary pozzolanic reactions. The analysis of the phase assemblages revealed characteristic crystalline products, including portlandite

and unhydrated clinker phases, primarily alite (C_3S), alongside the amorphous hump characteristic of C-S-H gel.

In the NS-OPC-PCE system, the diffractogram showed a pronounced diminution in peaks related to anhydrous C_3S, particularly the reflections at $2\theta \approx 29.4°$ and 32.2°. This observation strongly suggests a high degree of hydrated cement, which is due to the superior dispersive efficacy of the PCE superplasticizer. By electrosterically preventing the agglomeration of both cement grains and nano-silica particles, PCE facilitates greater access of water to the reactive clinker surfaces, thereby accelerating the hydration kinetics. More significantly, this sample exhibited the lowest peak intensities for portlandite, specifically at the principal (001) reflection plane at $2\theta \approx 18.1°$ and the (101) plane at $2\theta \approx 34.1°$. The substantial consumption of CH is a direct indicator of a vigorous reaction, where the well-dispersed, high-surface-area nano-silica reacts with the CH generated from clinker hydration. This pozzolanic activity densifies the microstructure by forming additional, secondary C-S-H, which is inferred from a subtle broadening of the amorphous halo centered around $2\theta \approx 29°$.

Conversely, the NS-OPC-KL specimen presented a markedly different mineralogical profile. The residual peaks for alite (C_3S) were significantly more prominent in this system compared to the PCE-modified counterpart, indicating a substantial fraction of unhydrated clinker even after 90 days of curing. This finding aligns with the well-documented retarding effect of lignosulfonates, where the lignin macromolecules attach onto the surfaces of cement colloids, impeding their dissolution and subsequent reaction with water. Consequently, the overall degree of hydration was suppressed. The intensity of the characteristic portlandite peaks in the KL system was considerably higher than in the PCE system, signifying a lower degree of CH consumption. Although Kraft lignin imparts some dispersive properties, its dominant chemical retardation mechanism appears to override the benefits of particle dispersion, resulting in a slower generation of CH and a kinetically hindered pozzolanic reaction. While both admixtures influence the composite's phase development, PCE promotes a highly efficient, well-hydrated, and pozzolanically active system. In contrast, Kraft lignin's inherent retarding nature leads to an incompletely reacted matrix with significantly reduced pozzolanic consumption of portlandite.

CH crystal size was also analysed using the Debye–Scherrer equation (Mustapha *et al.* 2019), based on FWHM values extracted from three key CH peaks at 18.0°, 34.1°, and 50.8°. These peaks were analyzed using Origin software to determine 2θ and FWHM values, which were then applied to the Debye–Scherrer formula:

$$D = \frac{\kappa \cdot \lambda}{\beta \cdot \cos\theta} \quad \ldots (2)$$

Here, DDD represents the crystallite size in nanometers, κ is the shape factor (commonly taken as 0.9), λ is the X-ray wavelength (1.5406 Å for Cu Kα radiation), β is the full width at half maximum expressed in radians, and θ is the Bragg diffraction angle. The incorporation of Kraft lignin-functionalized nano-silica (KL-NS) into the Ordinary Portland Cement (OPC) matrix was found to exert a profound influence on the crystallite habit of portlandite (CH). A significant reduction in the average CH crystal size was observed in the KL-NS-OPC composite when compared to both the plain OPC control and the NS-PCE-OPC formulation. For instance, quantitative analysis of the diffractograms revealed that the average CH crystallite dimension in the KL-NS-OPC sample was diminished by approximately 35.8% and 24.3% relative to the OPC and NS-PCE-OPC mixes, respectively. This crystal refinement is attributed to the adsorption of lignin macromolecules onto the nascent CH nucleation sites, which sterically hinders subsequent crystal growth and favors the formation of smaller, more numerous crystallites.

This downsizing of CH crystals is critical for enhancing the quality of the interfacial transition zone (ITZ) with the surrounding C-S-H gel (Wang *et al*. 2019). A finer CH0 crystal structure promotes superior stress transfer and mechanical interlocking at the microscopic level. Such microstructural densification is a key contributor to improved material cohesion and is directly correlated with an elevation in overall mechanical performance. Therefore, the strategic use of Kraft lignin-functionalized nano-silica provides a dual benefit: it not only reduces the total volume of CH through the pozzolanic reactivity of the nano-silica but also fundamentally refines the size and distribution of the remaining CH crystals. This combined effect yields a denser, more homogeneous, and ultimately more durable cementitious microstructure.

3.1.2 TG/DTG Analysis

An in-depth investigation into the thermal decomposition behavior of the nano-silica modified cementitious composites was conducted to compare the effects of a sustainable Kraft lignin (NS-KL) admixture against a conventional high-efficiency polycarboxylate ether (NS-PCE) superplasticizer. The analysis, using thermogravimetric (TG) and derivative thermogravimetric (DTG) techniques at 50 °C to 1000 °C, provides profound insights into how each admixture engineers a distinct microstructure with unique performance attributes. While both systems show

the viability of incorporating nano-silica, the thermal profiles reveal two divergent and sophisticated design philosophies: one targeting rapid reaction and the other, the NS-KL system, focusing on controlled kinetics and exceptional long-term resilience.

Results from ambient to 800 ℃ identified three principal mass-loss events. The first, below 200 ℃, corresponds to the dehydration of C-S-H and free water. The final event, above 600 ℃, is the decarbonation of calcium carbonate. The most diagnostically critical region, however, lies between 400 ℃ and 500 ℃, representing the dehydroxylation of portlandite (CH). It is here that the fundamental difference between the two systems is starkly revealed. The DTG curve for the NS-PCE sample exhibits a markedly suppressed CH peak, indicating a high degree of pozzolanic consumption. This demonstrates the exceptional efficiency of PCE in dispersing nano-silica, leading to a rapid and near-complete reaction that is ideal for applications requiring high early-age strength.

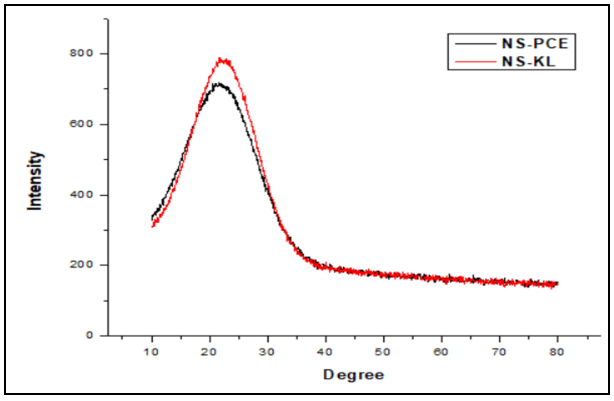


Fig. 2: XRD analyses of nano silica-PCE and nanosilica-kraft lignin cement specimens at 90 days

In stark contrast, the NS-KL composite displays a prominent and well-defined portlandite peak, signifying a substantially larger quantity of stable CH in the cured matrix. While the NS-PCE system prioritizes the rapid conversion of CH, the NS-KL system strategically retains it, creating a vital alkaline reservoir. This high alkalinity is the cornerstone of superior long-term durability, as it is essential for maintaining the passive, non-corroding oxide layer on embedded steel reinforcement, providing a robust defense against chloride-induced corrosion. This inherent chemical resilience, a direct result of the higher CH content, gives the NS-KL composite a clear advantage in structures designed for extended service life in aggressive environments.

This difference in phase assemblage is a direct consequence of the kinetic modulation imparted by the respective admixtures. PCE acts as a powerful accelerator for the hydration in cement composites. Conversely, the Kraft lignin macromolecules function as reaction modulators. This controlled hydration, unlike the highly accelerated kinetics of the PCE-based system, effectively mitigates the high exothermic heat of hydration, lowering the risk of cracking due to temperature gradients in bulk concrete. This makes the NS-KL system inherently more suitable for large-scale structural applications where thermal management is critical.

Furthermore, the two systems exhibit different trajectories for performance development. The NS-PCE system achieves a high degree of reaction quickly, with limited potential for further significant gains over time. The NS-KL system, however, is engineered for sustained, long-term improvement. Its microstructure, containing both a CH reserve and unreacted nano-silica, possesses a significant latent pozzolanic capacity. This allows the material to continue densifying its matrix, refining its pore structure, and increasing its strength and impermeability for decades. This ongoing reaction also imparts a potential for autogenous self-healing of micro-cracks, further enhancing its resilience. In conclusion, the TG/DTG analysis provides a compelling narrative of two distinct, high-performance materials. The NS-PCE system is optimized for rapid, high-efficiency reactions, while the NS-KL composite represents a more strategic approach, leveraging a sustainable admixture to create a material with a superior alkaline reserve for durability, controlled kinetics for safe application, and a latent capacity for lifelong performance enhancement.

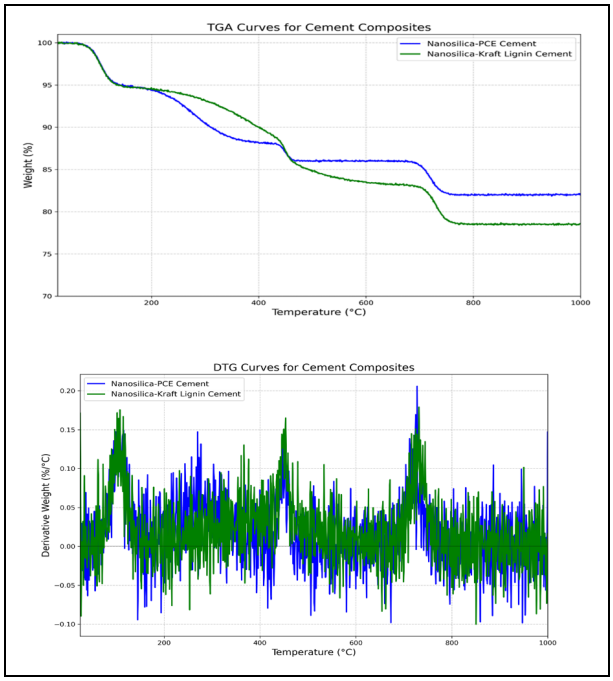


Fig. 3: TG/DTG curves of mixed specimens

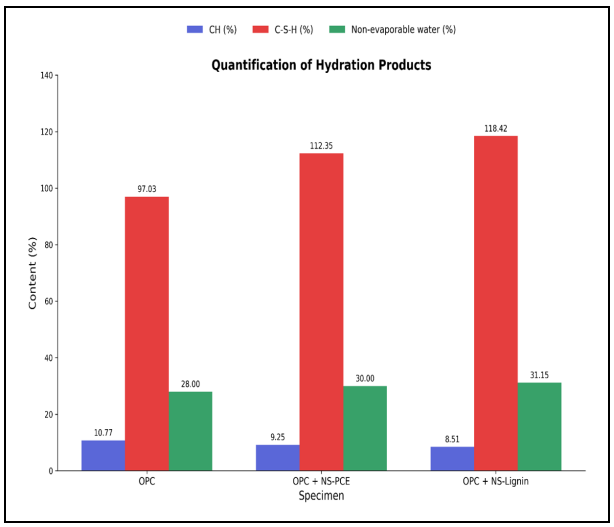


Fig. 4: CH, C–S–H, and non-evaporable water content of mix specimens

3.1.3 Mercury Intensity Porosimetry (MIP)

Effects of incorporating NS modified with PCE and KL admixture on the hydration chemistry and pore structure development of OPC composites reveal a complex and nuanced relationship between chemical reactivity and physical microstructural refinement. The quantitative analysis of hydration products, coupled with a detailed examination of the pore network topology, demonstrates that while both systems significantly enhance the cementitious matrix compared to a plain OPC control, they achieve this through fundamentally different mechanisms.

As estimated from the mass losses in the TG-DTG curves in Fig. 4, the residual CH content in the NS-PCE matrix was reduced to approximately 16%, a substantial decrease from the 22.5% observed in the plain OPC control. This efficient CH consumption directly fueled the formation of supplementary C-S-H, which reached a total content of roughly 68%, far exceeding the 59% in the control paste. This heightened performance is attributed to the exceptional dispersing capability of the PCE superplasticizer, which ensures a uniform deagglomeration of both cement and nano-silica particles, thereby maximizing the available reactive surface area and accelerating the pozzolanic reaction. The quantification of primary hydration products illustrated in Fig. 5 provides a clear measure of the pozzolanic efficiency within each system. The NS-PCE composite exhibited superior chemical reactivity, evidenced by the most significant consumption of calcium hydroxide (CH) and the highest production of calcium-silicate-hydrate (C-S-H) gel. While the NS-KL composite also demonstrated positive pozzolanic activity, its effects were more moderate. The CH content was reduced to an intermediate level of approximately 19%, with the corresponding C-S-H content increasing to 64% confirming that the reaction occurred but was kinetically hindered, a finding consistent with the well-documented retarding effect of lignin on cement hydration. From a purely chemical standpoint, the NS-PCE system appears to be the more potent formulation for generating the maximum volume of binding hydration products.

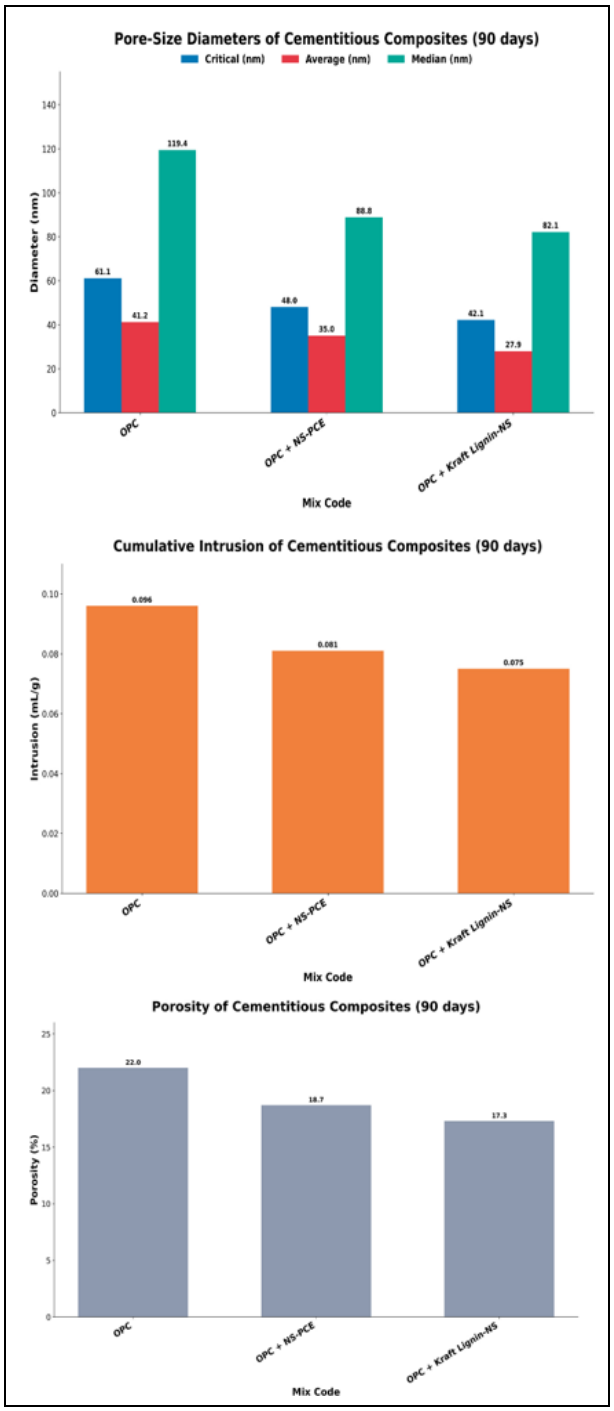


Fig. 5: Pore structure characteristics of mixed specimens

Table 5. Pore structure parameters for mixed specimens

Mix	Critical (nm)	Average (nm)	Median (nm)	Cumulative Intrusion (mL/g)	Porosity (%)
OPC	61.1	41.2	119.4	0.096	22
OPC + NS-PCE	48	35	88.8	0.081	18.7
OPC + Kraft Lignin-NS	42.1	27.9	82.1	0.075	17.3

However, the analysis of the pore structure depicted in Fig. 6 presents a counterintuitive and arguably more critical set of findings regarding the material's physical integrity. Table 5 highlights the pore structure parameters for the mix specimens. The primary objective of microstructural enhancement is the reduction of large, interconnected capillary pores, which are the most detrimental to strength and durability. In this respect, the NS-KL composite demonstrated a remarkable and superior performance. The fraction of harmful large capillary pores (0.1–10 μm) was dramatically reduced to just 39% of the total pore volume. This represents a profound improvement over the plain OPC (50%) and, significantly, is a more effective refinement than that achieved by the NS-PCE system, which retained a large pore fraction of 45%. This crucial finding suggests that sheer C-S-H volume does not solely govern pore refinement. The reduction in large pores in the NS-KL system was accompanied by a significant increase in the proportion of the smallest, harmless gel pores (<0.01 μm), which surged to over 12% of the total pore volume. This is nearly double the gel pore fraction found in the OPC control and substantially higher than the 8% achieved in the chemically efficient NS-PCE system.

These studies highlight that NS-PCE and NS-KL systems represent two distinct pathways to microstructural improvement. The NS-PCE system operates on a principle of high chemical efficiency, rapidly producing a large volume of C-S-H that densifies the matrix overall. In contrast, the NS-KL system's success lies in its superior physical refinement of the pore topology. The slower, controlled hydration kinetics modulated by the Kraft lignin likely allow the hydration products to precipitate more strategically within the larger voids of the developing pore network, effectively segmenting and blocking these harmful channels. Furthermore, the significant increase in gel pores suggests that the C-S-H formed in the presence of lignin may possess a different, possibly more voluminous or fibrillar morphology, or that the lignin macromolecules themselves become integrated into the pore walls, effectively refining the pore structure. Therefore, while the NS-PCE system excels in rapid, bulk densification, the NS-KL system demonstrates a more advanced level of pore engineering, creating a more tortuous and less permeable network.

3.1.4 SEM Analysis

A thorough microstructural examination of hardened cementitious composites, conducted via Scanning Electron Microscopy (SEM) after 90 days of curing, offers critical visual corroboration and novel insights into the distinct hydration and densification mechanisms influenced by various admixtures. Fig. 7(a-b) meticulously presents representative micrographs for a plain Ordinary Portland Cement (OPC) control, a nano-silica modified system utilizing polycarboxylate ether (NS-PCE), and a nano-silica system functionalized with Kraft lignin (NS-KL). These images collectively unravel the profound impact of each formulation on the morphology, distribution, and interconnectivity of hydration products, directly correlating with the bulk properties discussed from XRD, TG/DTG, and MIP analyses.

Fig. 7a, depicting the plain OPC control sample, reveals a relatively heterogeneous and porous microstructure. Prominent features include large, platy, and well-crystallized hexagonal flakes of calcium hydroxide (CH), often exceeding several micrometers in lateral dimension. These large CH crystals tend to form in interstitial spaces, creating weaker zones due to their preferred orientation and limited interfacial bonding with the surrounding C-S-H gel. Furthermore, the C-S-H morphology appears less refined, often presenting as a more open, porous network with visible gaps and unreacted cement particles still evident. This relatively coarse and less uniform distribution of hydration products in the control sample is characteristic of a standard hydration process without the benefits of advanced particle dispersion or enhanced pozzolanic activity. The presence of significant void spaces and a less dense matrix in the OPC control aligns perfectly with its higher porosity and larger pore diameters as quantified by MIP.

Meanwhile, Fig. 7b, showcasing the NS-PCE composite, illustrates a dramatically refined and densified microstructure. The most striking observation is the absence of large, well-defined CH crystals; instead,

only very fine, dispersed, or even amorphous CH phases are discernible, if at all. This visual evidence strongly supports the TG/DTG data, which indicated a significantly reduced CH content due to extensive pozzolanic consumption. C-S-H gel exhibits a dense, highly interlocked, and almost amorphous morphology, forming a continuous matrix that effectively encapsulates residual unreacted cement grains. The surface appears significantly smoother and more homogeneous compared to the OPC control, with a notable reduction in visible micro-cracks or large void spaces. The presence of highly densified C-S-H and minimal coarse CH directly contributes to the superior mechanical properties and reduced permeability associated with the NS-PCE system. This refined structure is due to the dispersing efficiency of PCE, which ensures fine NS particles act as nucleation sites for C-S-H growth and engage maximally in secondary pozzolanic reactions, effectively filling the inter-particle voids and creating a compact, cohesive matrix.

Fig. 7c, representing the NS-KL composite, offers a compelling visual narrative for the unique characteristics of the lignin-modified system. This image reveals a microstructure that, while distinct from both OPC and NS-PCE, is remarkably dense and uniform, particularly at the nanoscale. Unlike the large CH crystals in the OPC control, the CH in the NS-KL sample appears significantly reduced in size and more evenly distributed within the C-S-H matrix, often presenting as fine, dispersed crystallites. This observation visually confirms the reduction in CH crystal size and improved distribution inferred from previous analyses, attributing this to the specific interaction of lignin macromolecules with the CH growth mechanisms. The C-S-H gel in the NS-KL composite presents as a highly intricate, almost nano-fibrillar or nano-particulate network, characterized by exceptionally fine and densely packed agglomerates of hydration products. This morphology suggests that the Kraft lignin might influence the very growth habit of the C-S-H, with a greater proportion of smaller, more interconnected pores. The overall visual impression is one of a very tight, cohesive matrix, with a notable absence of large voids or macro-cracks. This highly refined pore architecture, particularly the abundance of smaller, gel-like phases and the effective filling of capillary voids, aligns perfectly with the MIP results, demonstrating superior pore refinement in the NS-KL system, especially the reduction in detrimental large capillary pores. The observed densification and uniform distribution of hydration products in the NS-KL sample underscore its potential for long-term durability and resistance to aggressive environmental ingress, validating its design as a material engineered for sustained performance and resilience.

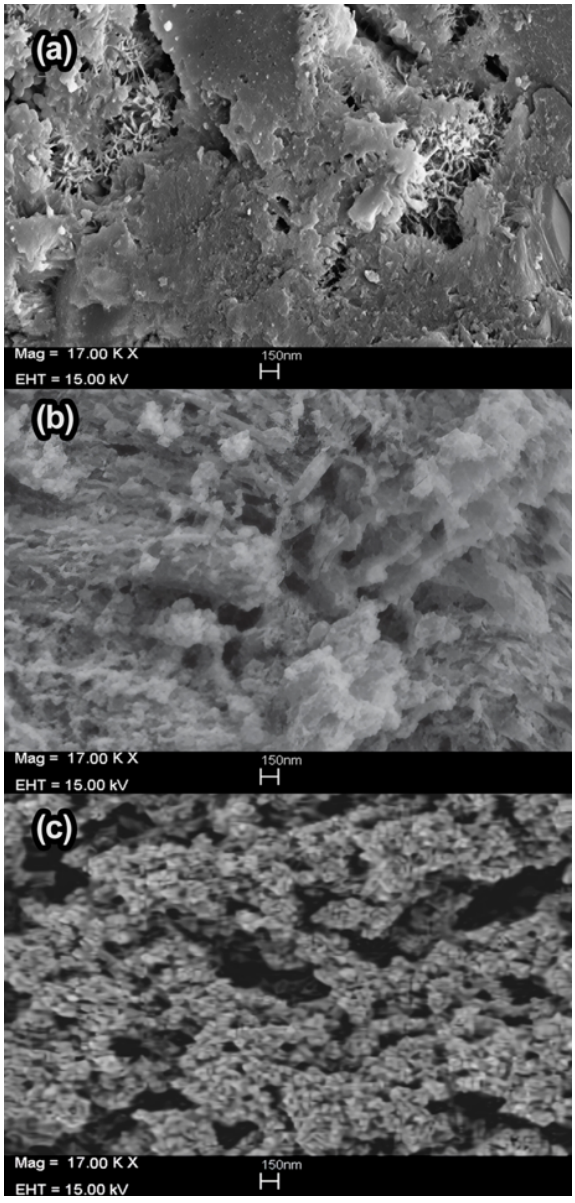


Fig. 6: SEM characterization of (a) control (OPC), (b) PCE-treated NS, and (C) kraft lignin-treated NS after 90 days

3.2 Macroscale Performance

3.2.1 Compressive strength

Compressive strength performance of the cementitious composites at 28 and 90 days is shown in Fig. 8. As anticipated, all mixtures exhibited a steady increase in strength with extended curing, which can be attributed to the ongoing hydration of cement clinker phases and, in the modified systems, the additional pozzolanic contribution of nanosilica. These processes promoted the progressive formation of binding gels such as C–A–S–H, C–S–H, and C–A–H, thereby enhancing the compactness and mechanical integrity of the matrix.

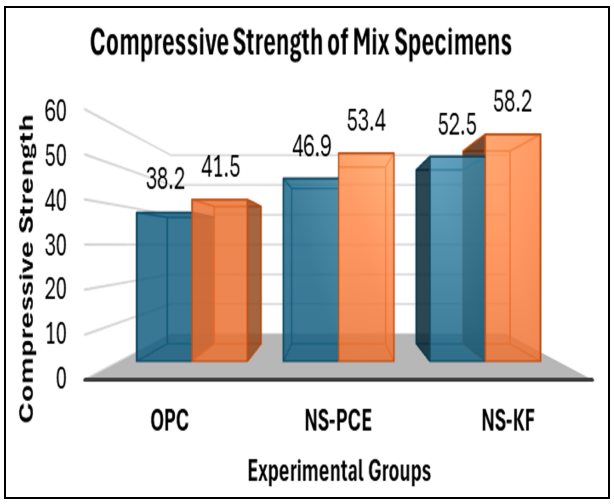


Fig. 7: Compressive strength of specimens at 28 and 90 days

Among the tested specimens, the Nano silica–Kraft Lignin–OPC mixture consistently outperformed the others. At 28 days, its compressive strength reached 52.5 MPa, which was approximately 37.4% higher than plain OPC (38.2 MPa) and 11.9% higher than the Nano silica–PCE–OPC blend (46.9 MPa). This advantage was maintained at 90 days, where the Kraft Lignin-modified system attained 58.2 MPa, surpassing OPC (41.5 MPa) by 40.2% and outperforming the PCE-based counterpart (53.4 MPa) by 9.0%. These results highlight the potential of Kraft Lignin as a surface modifier in synergy with nanosilica, providing superior strength enhancement compared to traditional PCE dispersants.

Statistical validation through ANOVA, summarized in Table 6, further supported these findings. At a 5% significance level ($\alpha = 0.05$), the mixtures incorporating nanosilica with either PCE or Kraft Lignin displayed F-values exceeding the critical threshold and P-values below 0.05, confirming that the observed strength improvements were statistically significant relative to plain OPC.

The superior performance of the Nano silica–Kraft Lignin–OPC blend can be attributed to several interrelated mechanisms (Xiaohan *et al*. 2024; Farzadnia *et al.* 2015; Regalla *et al.* 2024). Firstly, nanosilica acted as a filler, occupying voids and refining the pore network, while its high surface reactivity with calcium hydroxide, generating additional C–S–H gel. Secondly, well-dispersed nanosilica particles provided nucleation sites that accelerated hydration, contributing to both early- and later-age strength. Complementing these effects, Kraft Lignin imparted unique physicochemical functionality, enhancing nanosilica dispersion and imparting water-retentive properties that promoted internal curing. The sustained release of moisture helped to extend hydration, reduce unreacted cement content, and minimize early shrinkage and microcracking.

Overall, the combined benefits of nanosilica reactivity, microstructural densification, and the internal curing action of Kraft lignin produced a mechanically superior composite. These results demonstrate that Kraft lignin is more effective than conventional PCE in optimizing nanosilica dispersion and maximizing the strength development of cement-based materials.

3.2.2 UPV

Table 6. Compressive strength, UPV, electrical resistivity of OPC, nano silica–PCE–OPC, and kraft lignin–nanosilica–OPC specimens at 28 and 90 days

Property	Age (Days)	OPC	Nano Silica–PCE–OPC	OPC+Nano-silica+Kraft Lignin
Compressive Strength (MPa)	28	38.2	46.9	52.5
	90	41.5	53.4	58.2
UPV (m/s)	28	3687	4549	4950
	90	3886	4971	5480
Electrical Resistivity (kΩ·cm)	28	17.6	20.2	24.1
	90	19.7	23.1	27.8
F-value (CS)	28	—	23.4	31.2
	90	—	25.6	34.5
P-value (CS)	28	—	0.004	< 0.001
	90	—	0.003	< 0.001
F-value (UPV)	28	—	19.2	29.1
	90	—	21.5	32.7
P-value (UPV)	28	—	0.006	< 0.001
	90	—	0.005	< 0.001
F-value (ER)	28	—	16.8	25.8
	90	—	18.9	28.3
P-value (ER)	28	—	0.008	0.002
	90	—	0.007	< 0.001

Ultrasonic pulse velocity (UPV) results for the composites at 28 and 90 days are illustrated in Fig. 8. All mixtures showed higher UPV values with prolonged curing, reflecting the progressive hydration of clinker minerals in OPC and the additional pozzolanic contributions of nanosilica in the modified systems. These processes gradually improved the density and homogeneity of the cementitious matrix, enabling faster ultrasonic wave propagation. At 28 days, the UPV values for OPC, Nano silica–PCE–OPC, and Nano silica–Kraft Lignin–OPC were 3687, 4549, and 4950 m/s, respectively. By 90 days, the values increased to 3886, 4971, and 5480 m/s, corresponding to relative increments of approximately 5.4%, 9.3%, and 10.7% compared to their respective 28-day readings.

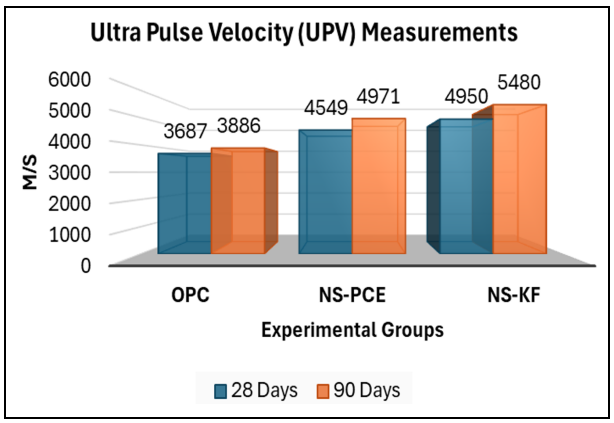


Fig. 8: UPV measurements of mix specimens

Among all specimens, the Nano silica–Kraft Lignin–OPC mixture consistently registered the highest UPV. At 90 days, its velocity was about 41.0% greater than plain OPC and 10.2% higher than the PCE-modified counterpart. The statistical analysis (Table 6) confirmed that these differences were significant, with F-values surpassing the critical limit and P-values below 0.05 at both curing ages.

The notable gains observed in the Kraft lignin system can be attributed to the combined actions of nanosilica and the lignin biopolymer. While nanosilica promoted microstructural densification through filler effects and nucleation sites, Kraft Lignin improved nanoparticle dispersion and contributed to a more uniform distribution of hydration products. Its ability to interact with water molecules likely delayed moisture loss, which helped sustain hydration reactions and reduced the formation of microcracks. This synergy resulted in a denser, more homogeneous matrix, as also supported by the microstructural features in Fig. 6(c).

According to Whitehurst's classification (Whitehurst, 1951), the OPC mixture was rated as good quality at both 28 and 90 days. In contrast, the Nano silica–PCE–OPC and Nano silica–Kraft Lignin–OPC composites were classified as excellent, owing to their superior compactness and reduced heterogeneity. These findings parallel the trends in compressive strength (Section 3.2.1), further highlighting the beneficial role of Kraft Lignin as a nanosilica modifier in cementitious composites.

3.2.3 Electrical Resistivity

Electrical resistivity testing was employed as a non-destructive means of characterizing the pore structure and transport resistance of the cementitious composites, since higher resistivity is generally associated with lower permeability and reduced ionic ingress (Tang *et al*. 2016). The results, presented in Fig. 9, show a consistent increase in resistivity from 28 to 90 days across all mixtures, in line with progressive hydration and pore refinement. At 28 days, the resistivity values were 3.687, 4.549, and 4.950 kΩ·cm for the OPC, Nano silica–PCE–OPC, and Nano silica–Kraft Lignin–OPC mixtures, respectively. By 90 days, these values rose to 3.886, 4.971, and 5.480 kΩ·cm, indicating respective gains of 5.4%, 9.3%, and 10.7% over their initial values.

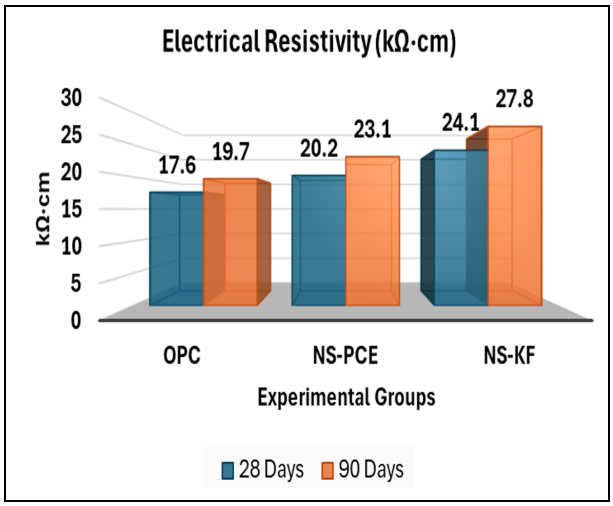


Fig. 9: Electrical resistivity measurements of mixed specimens

The Nano silica–Kraft Lignin–OPC composite consistently displayed the highest resistivity at both ages, suggesting the development of a more compact and impermeable microstructure compared with the other systems. At 90 days, its resistivity was 41.0% higher than that of OPC and 10.2% greater than that of the Nano silica–PCE–OPC blend. This superior performance can be attributed to the dual action of nanosilica and Kraft Lignin. While nanosilica enhanced hydration kinetics and consumed portlandite through pozzolanic activity, Kraft Lignin promoted better particle dispersion and contributed to a more homogeneous distribution of hydration products. Together, these effects reduced pore connectivity and refined the transport pathways available for ion migration.

Statistical validation through ANOVA confirmed the significance of these improvements, as the modified mixtures yielded F-values above the critical threshold and P-values below 0.05, confirming their resistivity enhancements over OPC were not random. Furthermore, the role of Kraft Lignin in suppressing microcrack formation and improving internal moisture management further reinforced the densification process, leading to a matrix with higher electrical resistivity. These results parallel the ultrasonic pulse velocity findings discussed in Section 3.2.2, underlining the positive influence of Kraft Lignin as a nanosilica modifier in improving durability-related properties.

4. CONCLUSION

This study investigated Kraft Lignin–modified nanosilica in cementitious composites, benchmarked against PCE-treated nanosilica and plain OPC using multi-scale experimental and statistical analyses. Microstructural results revealed enhanced nanosilica dispersion, accelerated portlandite consumption, increased C–S–H formation, and significant pore refinement, with ~31–32% reductions in pore sizes and ~21% lower porosity compared to OPC. These improvements translated into superior macro-scale performance, yielding higher compressive strength, UPV, and electrical resistivity at 90 days than both OPC and PCE–NS systems. ANOVA confirmed the statistical significance of all gains. Overall, Kraft Lignin proved to be an effective, sustainable alternative to synthetic PCE for high-performance cementitious composites.

FUNDING

This research received no specific grant from any funding agency in the public, commercial, or not-for-profit sectors.

CONFLICTS OF INTEREST

The authors declare that there is no conflict of interest.

COPYRIGHT

This article is an open-access article distributed under the terms and conditions of the Creative Commons Attribution (CC BY) license (http://creativecommons.org/licenses/by/4.0/).

REFERENCES

Alam, M. F., Shubham, K., Kumar, S. and Srivastava, A. K. L., Enhancing high-strength self-compacting concrete properties through Nano-silica: Analysis and prediction of mechanical strengths, *J. Build. Pathol. Rehabil.*, 9(1), 43 (2024). https://doi.org/10.1007/s41024-024-00386-7

Al-Abboodi, S. M. T., Al-Shaibani, E. J. A. and Alrubai, E. A., Preparation and characterization of nano silica prepared by different precipitation methods, *Conf. Ser.: Mater. Sci. Eng.*, 978(1), 012031 (2020). https://doi.org/10.1088/1757-899X/978/1/012031

ASTM C305-20 – Standard Practice for Mechanical Mixing of Hydraulic Cement Pastes and Mortars of Plastic Consistency. West Conshohocken, PA: ASTM International, (2020).

Argyropoulos, D. D. S., Crestini, C., Dahlstrand, C., Furusjö, E., Gioia, C., Jedvert, K., Henriksson, G., Hulteberg, C., Lawoko, M., Pierrou, C. and Samec, J. S., Kraft lignin: a valuable, sustainable resource, opportunities and challenges, *ChemSusChem*, 16(23), e202300492 (2023). https://doi.org/10.1002/cssc.202300492

Baten, B., Torsha, T. and Manzur, T., Corrosion vulnerability of reinforced concrete structures with different blended cement due to chloride ingress. *Mater. Today: Proc.*, 43, 1018-1024 (2021). https://doi.org/10.1016/j.matpr.2020.07.668

IS 13311 (Part 1):1992 – Non-destructive Testing of Concrete – Methods of Test, Part 1: Ultrasonic Pulse Velocity, New Delhi, BIS (1992.

IS 383:2016 – Coarse and Fine Aggregate for Concrete – Specification (3rd revision), New Delhi, BIS (2016.

IS 4031 (Part 6):1988 – Methods of Physical Tests for Hydraulic Cement, Part 6: Determination of Compressive Strength of Hydraulic Cement (other than masonry cement), New Delhi, BIS (1988.

IS 650:1991 – Specification for Standard Sand for Testing of Cement, New Delhi, BIS (1991.

IS 8112:2013 – Specification for 43 Grade Ordinary Portland Cement, New Delhi, BIS (2013).

Chen, J. J., Ng, P. L., Xu, L. and Kwan, A. K. H., Use of nano-silica sol in concrete: Performance and influence mechanisms, *Constr. Build. Mater.*, 411, 134582 (2024). https://doi.org/10.1016/j.conbuildmat.2023.134582

Chong, J. Z., Sutan, N. M. and Yakub, I., Characterization of early pozzolanic reaction of calcium hydroxide and calcium silicate hydrate for nanosilica modified cement paste, *J. Civil Eng., Sci. Technol.*, 4(3), 6-10 (2013). https://doi.org/10.33736/jcest.120.2013

Crestini, C., Lange, H., Sette, M. and Argyropoulos, D. S., On the structure of softwood kraft lignin, Green Chem., 19(17), 4104-4121 (2017). https://doi.org/10.1039/C7GC01812F

Dessbesell, L., Paleologou, M., Leitch, M., Pulkki, R. and Xu, C. C., Global lignin supply overview and kraft lignin potential as an alternative for petroleum-based polymers, *Renewable and Sustainable Energ. Rev.*, 123, 109768 (2020). https://doi.org/10.1016/j.rser.2020.109768

Farjad, P., Mehairi, A. G., Meshkani, F., Mowlaei, R., Khoshnazar, R. and Nassar, N. N., Compressive strength and microstructural development of cement paste incorporating nanosilica with different particle sizes, *CEMENT,* 19, 100128 (2025). https://doi.org/10.1016/j.cement.2025.100128

Farzadnia, N., Noorvand, H., Yasin, M. A. and Aziz, A. N. F., The effect of nano silica on short term drying shrinkage of POFA cement mortars, *Constr. Build. Mater.,* 95, 636-646 (2015). https://doi.org/10.1016/j.conbuildmat.2015.07.132

Feng, P., Chang, H., Liu, X., Ye, S., Shu, X. and Ran, Q., The significance of dispersion of nano-SiO2 on early age hydration of cement pastes, *Mater. Design*, 186, 108320 (2020). https://doi.org/10.1016/j.matdes.2019.108320

Gayathiri, K. and Praveenkumar. S., Elucidating the effects of dispersion methods on agglomerated nano silica particles in aqueous environment, *Materials Today: Proceedings*, (2023). https://doi.org/10.1016/j.matpr.2023.05.054

Gupta, C., Sverdlove, M. J. and Washburn, N. R., Molecular architecture requirements for polymer-grafted lignin superplasticizers, *Soft Matter*, 11(13), 2691-2699 (2015). https://doi.org/10.1039/C4SM02675F

Haruehansapong, S., Pulngern, T. and Chucheepsakul, S., Effect of the particle size of nanosilica on the compressive strength and the optimum replacement content of cement mortar containing nano-SiO2, *Const. Build. Mater.,* 50, 471-477 (2014). https://doi.org/10.1016/j.conbuildmat.2013.10.002

Hossain, M. M., Karim, M. R., Hasan, M., Hossain, M. K. and Zain, M. F. M., Durability of mortar and concrete made up of pozzolans as a partial replacement of cement: A review, *Constr. Build. Mater*., 116, 128-140 (2016). https://doi.org/10.1016/j.conbuildmat.2016.04.147

Huseien, G. F., A review on concrete composites modified with nanoparticles, *J. Compos. Sci*., 7(2), 67 (2023). https://doi.org/10.3390/jcs7020067

Iqbal, S., Pan, G., Meng, H., Sun, H., Liu, B. and Zhou, F., Surfactant-free synthesis of highly monodispersed in situ grown nano-silica on modified fly ash and its impact on the properties of cement pastes, *Constr. Build. Mater.,* 425, 136043 (2024). https://doi.org/10.1016/j.conbuildmat.2024.136043

Kaewunruen, S., Wu, L., Goto, K. and Najih, Y. M., Vulnerability of structural concrete to extreme climate variances, *Climate*, 6(2), 40 (2018). https://doi.org/10.3390/cli6020040

Kandasamy, A, Rachel, P. P., Khazaleh, M. A. and Athiappan, K., Comparative Analysis on Load-deformation Behavior of RC Slabs Incorporating Nano-SiO2 and Coconut Fibers, *J. Environ. Nanotechnol.,* 14(1), 18–29 (2025a). https://doi.org/10.13074/jent.2025.03.2511233

Kandasamy, A., Ramesh, B., Khazaleh, Al. M. and Athiappan, K., Behavior of High performance Geopolymer Concrete Beams with Substitution of Silica Fume and GGBS/Fly Ash, *J. Environ. Nano technol.,* 14(1), 52–62 (2025b). https://doi.org/10.13074/jent.2025.03.2511289

Kandasamy, A., Ramesh, B., Al Khazaleh, M. and Sabari, K., Evaluating the Microstructure and Strength of Geopolymer Mud Blocks for Sustainable Architecture, *Civil Eng. J.,* 11(4), 1410–1431 (2025c). https://doi.org/10.28991/CEJ-2025-011-04-09

Kalliola, A., Kangas, P., Winberg, I., Vehmas, T., Kyllönen, H., Heikkinen, J., Poukka, O., Kemppainen, K., Sjögård, P., Pehu-Lehtonen, L. and Liitiä, T., Oxidation process concept to produce lignin dispersants at a kraft pulp mill, *Nordic Pulp Pap. Res. J.,* 37(2), 394-404 (2014). https://doi.org/10.1016/j.conbuildmat.2013.10.002

Karamloo, M., Mazloom, M. and Payganeh, G., Influences of water to cement ratio on brittleness and fracture parameters of self-compacting lightweight concrete, *Eng. Fracture Mech.,* 168, 227-241 (2016). https://doi.org/10.1016/j.engfracmech.2016.09.011

Li, R., Chen, W. -C., Lei, L. and Plank, J., Dispersing efficacy of tailored IPEG PCEs in AAS binders: elucidating the impact of PCE molecular weight, *Ind. Eng. Chem. Res.,* 62(4), 1776-1787 (2023). https://doi.org/10.1021/acs.iecr.2c03820

Liu, B., Wang, L., Pan, G. and Li, D., Dispersion of graphene oxide modified polycarboxylate superplasticizer in cement alkali solution for improving cement composites, *J. Build. Eng.,* 57, 104860 (2022). https://doi.org/10.1016/j.jobe.2022.104860

Lv, S., Liang, S., Zuo, J., Zhang, S., Wang, J. and Wei, D., Lignin-based anti-UV functional materials: recent advances in preparation and application, *Iran. Polym. J.,* 32(11), 1477-1497 (2023). https://doi.org/10.1007/s13726-023-01218-0

Mahmood, F. S., Hussein, H. Q. and Abdulwahhab, Z. T. Preparation and characterization of high surface area nanosilica from Iraqi sand via sol-gel technique, *J. Petrol. Res. Stud.,* 12(4), 104-117 (2022). https://doi.org/10.52716/jprs.v12i4.645

Mustapha, S., Ndamitso, Abdulkareem, A. S., Tijani, J. O., Shuaib, D. T., Mohammed, A. K. and Sumaila, A., Comparative study of crystallite size using Williamson-Hall and Debye-Scherrer plots for ZnO nanoparticles, *Adv. Nat. Sci.: Nanosci. Nanotechnol*., 10(4), 045013 (2019). https://doi.org/10.1088/2043-6254/ab52f7

Naddaf, M., Kafa, H. and Ghanem, I., Extraction and characterization of nano-silica from olive stones, *Silicon,* 12, 185-192 (2020). https://doi.org/10.1007/s12633-019-00112-w

Paul, S. C., Rooyen, V. A. S., Zijl, V. G. P. and Petrik, L. F., Properties of cement-based composites using nanoparticles: A comprehensive review, *Constr. Build. Mater.,* 189, 1019-1034 (2018). https://doi.org/10.1016/j.conbuildmat.2018.09.062

Pooja, D., Nagarajan, M. and Thangasamy, L., Assessing the Durability, Mechanical, and Microstructural Properties of Nanosilica-enhanced Coconut Shell Concrete: A Sustainable Approach, *J. Environ. Nanotechnol.,* 13(3), 237-245 (2024). https://doi.org/10.13074/jent.2024.09.243845

Prasad, V., Siddiqui, L., Mishra, P.K., Ekielski, A. and Talegaonkar, S., Recent advancements in lignin valorization and biomedical applications: a patent review, *Recent Pat. Nanotechnol*., 16(2), 107-127 (2022). https://doi.org/10.2174/1872210515666210216085831

Puttbach, C., Prinz, G. S. and Murray, C. D. Strength and stiffness characterization of ultra-high performance concrete (UHPC) cement paste phases through in-situ micro-mechanical testing, *Cem. Concr. Compos*., 149, 105520 (2024). https://doi.org/10.1016/j.cemconcomp.2024.105520

Qian, Y, Lesage, K., El Cheikh, K. and Schutter, D. G., Effect of polycarboxylate ether superplasticizer (PCE) on dynamic yield stress, thixotropy and flocculation state of fresh cement pastes in consideration of the Critical Micelle Concentration (CMC), *Cem. Concr. Res.,* 107, 75-84 (2018). https://doi.org/10.1016/j.cemconres.2018.02.019

Quercia, G., Lazaro, A., Geus, J. W. and Brouwers, H. J. H., Characterization of morphology and texture of several amorphous nano-silica particles used in concrete, *Cem. Concr. Compos*., 44, 77-92 (2013). https://doi.org/10.1016/j.cemconcomp.2013.05.006

Rajagopalan, N., Winberg, I., Fearon, O., Cardellini, G., Liitia, T. and Kalliola, A., Environmental Performance of Oxidized Kraft Lignin-Based Products, *Sustainability,* 14(17), 10897 (2022). https://doi.org/10.3390/su141710897

Regalla, S. S. and Kumar, S., Effect of nano SiO2 on rheology, nucleation seeding, hydration mechanism, mechanical properties and microstructure amelioration of ultra-high-performance concrete, *Case Stud. Constr. Mater.,* 20, e03147 (2024). https://doi.org/10.1016/j.cscm.2024.e03147

Ren, C., Hou, L., Li, J., Lu, Z. and Niu, Y., Preparation and properties of nanosilica-doped polycarboxylate superplasticizer, *Constr. Build. Mater*., 252, 119037 (2020). https://doi.org/10.1016/j.conbuildmat.2020.119037

Rupasinghe, M., Nicolas, S. R., Mendis, P., Sofi, M. and Ngo, T., Investigation of strength and hydration characteristics in nano-silica incorporated cement paste, *Cem. Concr. Compos.,* 80, 17-30 (2017). https://doi.org/10.1016/j.cemconcomp.2017.02.011

Sabari, K., Muniappan, A., Deepanraj, B. and Mohamed, S. J. M., Enhancing Mechanical Performance of Friction Stir Welded AZ31 Magnesium Alloy with Nano-TiC Reinforcements Using Grey Relational Analysis, *Int. J. Precis. Eng. Manuf.,* 26, 27–41 (2025). https://doi.org/10.1007/s12541-024-01096-3

Shah, S. P., Hou, P. and Cheng, X., Durability of cement-based materials and nano-particles: a review, Proceedings of NICOM5, *Springer Cham*, 15-24 (2015). https://doi.org/10.1007/978-3-319-17088-6_2

Tang, S. W., Cai, X. H., He, Z., Zhou, W., Shao, H. Y., Li, Z. J., Wu, T. and Chen, E., The review of pore structure evaluation in cementitious materials by electrical methods, *Constr. Build. Mater.,* 117, 273-284 (2016). https://doi.org/10.1016/j.conbuildmat.2016.05.037

Wang, H. M., Yuan, T. Q., Song, G. Y. and Sun, R. C., Advanced and versatile lignin-derived biodegradable composite film materials toward a sustainable world, *Green Chem.,* 23(11), 3790-3817 (2021). https://doi.org/10.1039/D1GC00790D

Wang, J., Jiaxin, L., Xiangming, K. and Yin, Y., Characterization of the nanoparticles formed in aqueous phase of hydrating cement pastes in the presence of PCEs, *Cem. Concr. Res.,* 165, 107087 (2023). https://doi.org/10.1016/j.cemconres.2022.107087

Wang, Q, Li, S., Pan, S., Cui, X., Corr, D. J. and Shah, P. S., Effect of graphene oxide on the hydration and microstructure of fly ash-cement system, *Constr. Build. Mater.* 198, 106-119 (2019). https://doi.org/10.1016/j.conbuildmat.2018.11.199

Whitehurst, E. A., Soniscope tests con crete structures, In *J. Proc.,* 47(2), 433-444 (1951). https://doi.org/10.14359/12004

Xiaohan, Z., Ahmad, J., Mohammed, Y. J. and Farouk, A. D., A review on partial substitution of nanosilica in concrete, *Rev. Adv. Mater. Sci.,* 63(1), 20230157 (2024). https://doi.org/10.1515/rams-2023-0157

Xu, Z., Zhou, Z., Du, P. and Cheng, X., Effects of nano-silica on hydration properties of tricalcium silicate, *Constr. Build. Mater.,* 125, 1169-1177 (2016). https://doi.org/10.1016/j.conbuildmat.2016.09.003

Yang, T., Liu, B., Li, L., Gan, X., Lu, L. and Li, Y., Agglomeration behavior of colloidal nano-silica and its effect on pore structure, mechanical properties and shrinkage of cement mortar, *Constr. Build. Mater.,* 409, 133865 (2023). https://doi.org/10.1016/j.conbuildmat.2023.133865

Yim, H. J., Lee, H., and Kim, H. J., Evaluation of mortar setting time by using electrical resistivity measurement, *Constr. Build. Mater.,* 146, 679-686 (2017). https://doi.org/10.1016/j.conbuildmat.2017.04.088

Zandonadi N. C. C., de Paula, H. B., Demuner, I. F., de Paula, M. O., Pedroti, L. G. and Carvalho, A. M. M. L., Kraft lignin biorefinery: from pulping side streams to concrete plasticizers, *Europ. J. Wood Prod.,* 82(3), 849-860 (2024). https://doi.org/10.1007/s00107-024-02044-8

Zhang, J., Wang, Q. and Wang, Z., Optimizing design of high strength cement matrix with supplementary cementitious materials, *Constr. Build. Mater*., 120, 123-136 (2016). https://doi.org/10.1016/j.conbuildmat.2016.05.100

Zhang, Y. and Naebe, M., Lignin: A review on structure, properties, and applications as a light-colored UV absorber, *ACS Sustainable Chem. Eng*., 9(4), 1427-1442 (2021). https://doi.org/10.1021/acssuschemeng.0c06998

Zheng, T., Zhong, D., Zheng, D., Bao, F., Zheng, J. and Qiu, X., Kraft lignin grafted with isopentenol polyoxyethylene ether and the dispersion performance*, Int. J. Biol. Macromol.,* 150, 1147-1154 (2020). https://doi.org/10.1016/j.ijbiomac.2019.10.122

Zhou, X. F. and Lu, X. J., Structural characterization of kraft lignin for its green utilization, *Wood Res.,* 59(4), 583-592 (2014).